Comput Mech (2008) 43:61–72
DOI 10.1007/s00466-008-0255-5

ORIGINAL PAPER

# Fixed-point fluid–structure interaction solvers with dynamic relaxation

**Ulrich Küttler · Wolfgang A. Wall**

Received: 31 October 2007 / Accepted: 20 January 2008 / Published online: 22 February 2008


**Abstract** A fixed-point fluid–structure interaction (FSI) solver with dynamic relaxation is revisited. New developments and insights gained in recent years motivated us to present an FSI solver with simplicity and robustness in a wide range of applications. Particular emphasis is placed on the calculation of the relaxation parameter by both Aitken's $\Delta^2$ method and the method of steepest descent. These methods have shown to be crucial ingredients for efficient FSI simulations.

**Keywords** Fluid–structure interaction · Fixed-point solver · Dirichlet–Neumman partitioning · Strong coupling

## 1 Introduction

The development of numerical solvers for fluid–structure interaction (FSI) problems has been an active area of research in the last decade. Reliable FSI solvers are demanded in areas as diverse as aeroelasticity [8,21], civil engineering [41] or hemodynamics [2,16]. And as wide as the possible field of application are the requirements the solvers are confronted with: aerodynamics applications can couple a light compressible fluid to a stiff structure (e.g. aircraft wing) or a light incompressible fluid to a very light structure (e.g. parachute or sail), whereas hemodynamics simulations couple incompressible fluids and flexible structures with very comparable density. Thus there cannot be one FSI solver that fits all needs. Instead a variety of solution procedures is needed.

A particular interesting class of FSI problems, that is the appropriate model in many areas, is the interaction of incompressible fluids with structures that undergo large deformations. In that case both fields, the fluid and the structure, present computational challenges on their own. And still the coupling is a nontrivial task, as the large structural deformations have a huge impact on the fluid field's size and the coupled solution. Oftentimes there are sophisticated field solvers available that should be reused. This presents a further constraint to a possible coupling scheme. There are, of course, monolithic solvers that treat the nonlinear coupled problem in one go [2,18,19,36], however these approaches require access to the field solver internals and cannot be pursued with black box solvers. The same goes for partitioned approaches that mimic the behavior of monolithic solvers [7].

One possible partitioning strategy that enables the reuse of existing field solvers is the Dirichlet–Neumann partitioning, the predominant partition approach for FSI solvers. The most popular coupling methods are fixed-point methods [27,30,40] and interface Newton Krylov methods [10,15,16]. Other solvers suggested include a block-Newton solver with finite differenced off-diagonal blocks [25] and solvers based on vector extrapolation methods [26,37]. See also [33,34] for a FSI solver framework that includes partitioned block-iterative and quasi-direct coupling solvers as well as monolithic solvers.

The most basic and yet highly efficient approach among this variety of methods is the fixed-point method with dynamic relaxation as suggested in [27,40]. It is extremely easy to implement and surprisingly efficient and robust. Hence, in many cases this is the method of choice and it is an especially preferred method to use if a new attempt at FSI or other coupled problems is pursued. Unfortunately, however, the method has never been published in a journal but only in two hardly available conference proceedings [27,40] so far. This paper finally provides the detailed treatment of both the Aitken relaxation method and the relaxation via the method

U. Küttler · W. A. Wall (✉)
Chair of Computational Mechanics, TU Munich,
Boltzmannstr. 15, 85747 Garching, Germany
e-mail: wall@lnm.mw.tum.de

of steepest descent in the context of fixed-point iteration FSI solvers. We attempt to give as easy an introduction as possible. Yet this is not meant to be a mere reiteration of the original work [27]. The continuous work on FSI problems and the ever growing number of FSI solvers stimulated a subtle change of perception that is reflected in the present contribution. Nowadays there is much more emphasize on the formulation of the nonlinear interface problem that is amenable to many nonlinear solution approaches. The nonlinear field solvers are placed behind the opaque interface equation to keep them separated from the coupling algorithm.

The remainder of this paper is organized as follows: In Sect. 2 the field equations and coupling conditions of the FSI problem are presented. The introduction of the fixed-point solver with Dirichlet–Neumann partitioning follows in Sect. 3 and details on the available relaxation methods are presented in Sect. 4. Finally two examples are shown in Sect. 5.

## 2 Field equations

The FSI problem domain consists of the nonoverlapping fluid and structural domains $\Omega^F$ and $\Omega^S$. Both share a common interface $\Gamma$. In case of an incompressible fluid interacting with an elastic body the velocity $\mathbf{u}$ and the pressure $p$ are chosen for the unknowns of the fluid field, whereas the structural field unknown is the displacement $\mathbf{d}$.

### 2.1 Coupling conditions

Essential for the interaction of both fields is the coupling of the field variables at the interface. Both kinematic and dynamic continuity need to be fulfilled at all times. In the usual case of non-slip conditions at the interface this amounts to

$$\mathbf{u}_\Gamma = \frac{\mathrm{d}\mathbf{d}_\Gamma}{\mathrm{d}t} \quad \text{and} \quad \boldsymbol{\sigma}^S_\Gamma \cdot \mathbf{n} = \boldsymbol{\sigma}^F_\Gamma \cdot \mathbf{n} \tag{1}$$

where of course the interface displacement $\mathbf{d}_\Gamma$ does change the interface position $\mathbf{x}_\Gamma = \mathbf{x}_{0,\Gamma} + \mathbf{d}_\Gamma$ relative to the starting position $\mathbf{x}_{0,\Gamma}$. Therefore kinematic continuity states that along with the interface velocity $\mathbf{u}_\Gamma$ of the fluid field the whole fluid domain $\Omega^F$ changes in time. The dynamic continuity states that the stresses equal at the deformed interface where $\mathbf{n}$ constitutes the time dependent interface normal.

### 2.2 Structural domain

The structural displacements $\mathbf{d}$ are governed by the geometrically nonlinear elastodynamics equations

$$\rho^S \frac{\mathrm{d}^2\mathbf{d}}{\mathrm{d}t^2} = \nabla \cdot (\mathbf{F} \cdot \mathbf{S}) + \rho^S \mathbf{b}^S \quad \text{in } \Omega^S \times (0,T), \tag{2}$$

where $\rho^S$ and $\mathbf{b}^S$ represent the structural density and specific body force, respectively. The second Piola-Kirchhoff stress tensor $\mathbf{S}$ is related to the Green-Lagrangian strains via

$$\mathbf{S} = \mathbf{C} : \mathbf{E} \quad \text{with} \quad \mathbf{E} = \frac{1}{2}\left(\mathbf{F}^T \cdot \mathbf{F} - \mathbf{I}\right), \tag{3}$$

where $\mathbf{C}$ denotes the material tensor and $\mathbf{F} = \nabla\mathbf{d}$ represents the deformation gradient. The time dependent problem (2) is subject to the initial and boundary conditions

$$\mathbf{d} = \mathbf{d}_0 \quad \text{and} \quad \frac{\mathrm{d}\mathbf{d}}{\mathrm{d}t} = \frac{\mathrm{d}\mathbf{d}_0}{\mathrm{d}t} \quad \text{in } \Omega^S \text{ at } t = 0$$
$$\mathbf{d} = \bar{\mathbf{d}} \quad \text{on } \Gamma^S_D, \qquad \mathbf{S} \cdot \mathbf{n} = \bar{\mathbf{h}}^S \quad \text{on } \Gamma^S_N,$$

where $\Gamma^S_D$ and $\Gamma^S_N$ denote the Dirichlet and Neumann partition of the structural boundary, respectively.

### 2.3 Fluid domain

Fluid velocity $\mathbf{u}$ and pressure $p$ are governed by the incompressible Navier-Stokes equations

$$\frac{\partial\mathbf{u}}{\partial t} + \mathbf{u}\cdot\nabla\mathbf{u} - \frac{1}{\rho^F}\nabla\cdot\boldsymbol{\sigma}^F = \mathbf{b}^F \quad \text{in } \Omega^F \times (0,T), \tag{4}$$

$$\nabla\cdot\mathbf{u} = 0 \quad \text{in } \Omega^F \times (0,T). \tag{5}$$

The vector field $\mathbf{b}^F$ denotes the specific body force and $\rho^F$ the density of the fluid. In case of FSI simulations the fluid domain $\Omega^F$ varies in time due to the moving interface $\Gamma$. One way to account for the domain changes is to consider the whole fluid domain to deform continuously, starting with interface displacement $\mathbf{d}_\Gamma$. That is to prescribe a unique mapping

$$\mathbf{x} = \varphi(\mathbf{d}_\Gamma, \mathbf{x}_0, t) \tag{6}$$

of the fluid domain which matches the interface displacements. This mandates an arbitrary Lagrangian-Eulerian (ALE) formulation [9,12] of the Navier-Stokes equations and (4) changes to

$$\left.\frac{\partial\mathbf{u}}{\partial t}\right|_{\mathbf{x}_0} + \mathbf{c}\cdot\nabla\mathbf{u} - \frac{1}{\rho^F}\nabla\cdot\boldsymbol{\sigma}^F = \mathbf{b}^F \quad \text{in } \Omega^F \times (0,T). \tag{7}$$

The ALE-convective velocity is given as $\mathbf{c} = \mathbf{u} - \mathbf{u}^G$, with the domain velocity $\mathbf{u}^G = \partial\varphi/\partial t$. The stress tensor of a Newtonian fluid is given by

$$\boldsymbol{\sigma}^F = -p\mathbf{I} + 2\mu\boldsymbol{\epsilon}(\mathbf{u}) \quad \text{where} \quad \boldsymbol{\epsilon}(\mathbf{u}) = \frac{1}{2}\left(\nabla\mathbf{u} + \nabla\mathbf{u}^T\right) \tag{8}$$

denotes the strain rate tensor and $\mu$ the viscosity. The kinematic viscosity is given by $\nu = \mu/\rho^F$.

The partial differential equation (7) is subject to the initial and boundary conditions

$$\mathbf{u} = \mathbf{u}_0 \quad \text{in } \Omega^F \text{ at } \quad t = 0$$
$$\mathbf{u} = \bar{\mathbf{u}} \quad \text{on } \Gamma^F_D, \qquad \boldsymbol{\sigma}^F \cdot \mathbf{n} = \bar{\mathbf{h}}^F \quad \text{on } \Gamma^F_N. \tag{9}$$

### 2.4 Coupled FSI system

A proper discretization in space and time of equations (2), (5) and (7) and a particular version of the fluid domain mapping (6) together with discrete versions of the coupling conditions (1) lead the following nonlinear system of algebraic equations

$$\mathbf{F}\left(\mathbf{u}^{n+1}, p^{n+1}, \mathbf{d}^{G,n+1}\right) = \mathbf{f}^F \tag{10}$$

$$\mathbf{S}\left(\mathbf{d}^{n+1}\right) = \mathbf{f}^S \tag{11}$$

$$\mathbf{M}\left(\mathbf{d}^{G,n+1}\right) = \mathbf{0} \tag{12}$$

$$\mathbf{C}_{SF}\left(\mathbf{d}_\Gamma^{n+1}, \mathbf{u}_\Gamma^{n+1}, p^{n+1}\right) = \mathbf{0} \tag{13}$$

$$\mathbf{C}_{SM}\left(\mathbf{d}_\Gamma^{n+1}, \mathbf{d}_\Gamma^{G,n+1}\right) = \mathbf{0} \tag{14}$$

where $\mathbf{d}^{G,n+1}$ constitutes the fluid mesh movement and the coupling $\mathbf{C}_{SF}$ between structure and fluid and the coupling $\mathbf{C}_{SM}$ between structure and mesh describe conditions to be met at the interface.

It is understood that all operators depend on the current time step $n+1$. The spatial discretization of all fields is done using finite elements. In detail these operators are:

– Fluid $\mathbf{F}\left(\mathbf{u}^{n+1}, p^{n+1}, \mathbf{d}^{G,n+1}\right) = \mathbf{f}^F$:
With one-step-$\theta$ time discretization, for simplicity of presentation, the discrete version of Navier-Stokes is

$$\begin{bmatrix} \frac{1}{\Delta t}\mathbf{M}^F + \theta\left(\mathbf{N}^F(\mathbf{u}^{n+1}) + \mathbf{K}^F\right) & \theta\mathbf{G} \\ \theta\mathbf{G}^T & \mathbf{0} \end{bmatrix} \begin{bmatrix} \mathbf{u}^{n+1} \\ \mathbf{p}^{n+1} \end{bmatrix} = \begin{bmatrix} \mathbf{b}^F + (1-\theta)\,\mathbf{M}^F\dot{\mathbf{u}}^n + \frac{1}{\Delta t}\mathbf{M}^F\mathbf{u}^n \\ \mathbf{0} \end{bmatrix} \tag{15}$$

where the integration has to be performed on a time varying domain $\Omega^F(t)$, that is all terms depend on the mesh deformation $\mathbf{d}^{G,n+1}$.

*Remark 1* Additional stabilization terms are required in equation (15). For brevity these terms are not considered here. See [14] for a throughout discussion of stabilized finite elements for flow calculations.

– Structure $\mathbf{S}\left(\mathbf{d}^{n+1}\right) = \mathbf{f}^S$:
Discretized in time using the generalized-$\alpha$ method [4] the structural equations read

$$\begin{aligned} &\frac{1-\alpha_m}{\beta\Delta t^2}\mathbf{M}^S\mathbf{d}^{n+1} + (1-\alpha_f)\mathbf{f}_{int}(\mathbf{d}^{n+1}) \\ &\quad = (1-\alpha_f)\mathbf{f}_{ext}^{n+1} + \alpha_f\mathbf{f}_{ext}^n \\ &\qquad + \mathbf{M}^S\left(\frac{1-\alpha_m}{\beta\Delta t^2}\mathbf{d}^n + \frac{1-\alpha_m}{\beta\Delta t}\dot{\mathbf{d}}^n + \frac{1-\alpha_m-2\beta}{2\beta}\ddot{\mathbf{d}}^n\right) \\ &\qquad - \alpha_f\mathbf{f}_{int}(\mathbf{d}^n). \end{aligned} \tag{16}$$

– Mesh $\mathbf{M}(\mathbf{d}^{G,n+1}) = \mathbf{0}$:
A simple linear mesh equation might look like this

$$\mathbf{K}^M\mathbf{d}^{G,n+1} = \mathbf{f}^M\left(\mathbf{d}_\Gamma^{n+1}\right) \tag{17}$$

where $\mathbf{f}^M(\mathbf{d}_\Gamma^{n+1})$ stems only from the prescribed interface displacement $\mathbf{d}_\Gamma^{n+1}$ and $\mathbf{K}^M$ is an arbitrary operator that extends the interface displacement to the interior of the fluid domain.

The coupling Eqs. (13) and (14) are couplings that apply at the FSI interface only. There are sophisticated mortar methods available to couple various sorts of meshes, see e.g. [28]. The simplest coupling possible, however, is the coupling of matching meshes where all coupling operators $\mathbf{C}$ simplify to diagonal matrices at the FSI interface. For simplicity only matching meshes are considered here.

– Structure to fluid coupling $\mathbf{C}_{SF}(\mathbf{d}_\Gamma^{n+1}, \mathbf{u}_\Gamma^{n+1}) = \mathbf{0}$:

$$\mathbf{u}_\Gamma^{n+1} = \frac{\mathbf{d}_\Gamma^{n+1} - \mathbf{d}_\Gamma^n}{\Delta t} \tag{18}$$

– Structure to mesh coupling $\mathbf{C}_{SM}(\mathbf{d}_\Gamma^{n+1}, \mathbf{d}_\Gamma^{G,n+1}) = \mathbf{0}$:

$$\mathbf{d}_\Gamma^{G,n+1} = \mathbf{d}_\Gamma^{n+1} \tag{19}$$

*Remark 2* The mesh deformation equation (12) is coupled to the structural equation (11), but not vice versa. So the structural deformation is (of course) not retained by the mesh equation, but the structure drags the mesh along.

## 3 Dirichlet–Neumann coupling scheme

The system (10)–(14) constitutes a coupled set of nonlinear algebraic equations to be solved once for each time step. A Dirichlet–Neumann partitioning can be applied to solve this system, where the fluid field becomes the Dirichlet partition with prescribed interface velocities $\mathbf{u}_\Gamma^{n+1}$ and the structural field becomes the Neumann partition loaded with interface forces $\mathbf{f}_\Gamma^{F,n+1}$. This way the field solvers remain independent of each other and black box solvers can be used.

The particular advantage of a Dirichlet–Neumann coupling for FSI problems comes from the deformation of the fluid domain $\Omega^F$. The unknown interface displacements $\mathbf{d}_\Gamma^{n+1}$ determine shape and size of the fluid domain $\Omega^F$, thus the Navier-Stokes equation (15) has to be solved on a domain the size of which depends on the unknown solution. This difficulty of a free boundary value problem arises independent of the particular mesh moving scheme (17), even independent of how the changing fluid domain is described numerically,

e.g. via moving or fixed grids [31,32,35,39]. Many fluid solvers are unable to solve such free boundary value problems. The Dirichlet–Neumann partitioning, however, cures this problem by prescribing definite interface displacements $\mathbf{d}_\Gamma^{n+1}$ to the fluid solver. So the Navier-Stokes equation (15) needs to be solved on a domain with prescribed motion. The remaining fluid field unknowns are velocity $\mathbf{u}^{n+1}$ and pressure $p^{n+1}$.

### 3.1 Solver coupling

A detailed discussion of the solver coupling in a Dirichlet–Neumann partitioning requires to distinguish between interior degrees of freedom $I$ and degrees of freedom at the coupling interface $\Gamma$. With this distinction the structural equation $\mathbf{S}\left(\mathbf{d}^{n+1}\right) = \mathbf{f}^S$ reads

$$\begin{bmatrix} \mathbf{S}_{II} & \mathbf{S}_{I\Gamma} \\ \mathbf{S}_{\Gamma I} & \mathbf{S}_{\Gamma\Gamma} \end{bmatrix} \begin{bmatrix} \mathbf{d}_I \\ \mathbf{d}_\Gamma \end{bmatrix} = \begin{bmatrix} \mathbf{f}_I^S \\ \mathbf{f}_\Gamma^S \end{bmatrix}. \tag{20}$$

The same applies to the mesh and the fluid equation as well. However, in case of the fluid equations all pressure degrees of freedom belong to the domain's interior and are subsumed in the variable $\mathbf{u}_I$ in the further notation. Furthermore due to the Dirichlet–Neumann coupling the fluid mesh displacement $\mathbf{d}^{G,n+1}$ is known during the fluid solver execution. So the fluid operator turns into

$$\begin{bmatrix} \mathbf{F}_{II} & \mathbf{F}_{I\Gamma} \\ \mathbf{F}_{\Gamma I} & \mathbf{F}_{\Gamma\Gamma} \end{bmatrix} \begin{bmatrix} \mathbf{u}_I \\ \mathbf{u}_\Gamma \end{bmatrix} = \begin{bmatrix} \mathbf{f}_I^F \\ \mathbf{f}_\Gamma^F \end{bmatrix}. \tag{21}$$

With these definitions details of the solver coupling can be given:

1. Start with a suitably predicted interface displacement $\mathbf{d}_\Gamma^{n+1}$.
2. Solve mesh equation

$$\mathbf{M}_{II}\mathbf{d}_I^{G,n+1} = -\mathbf{M}_{I\Gamma}\mathbf{d}_\Gamma^{G,n+1} \tag{22}$$

with interface condition $\mathbf{d}_\Gamma^{G,n+1} = \mathbf{d}_\Gamma^{n+1}$ and calculate resulting grid and interface velocity (see [11,12]).

$$\mathbf{u}^{G,n+1} = \frac{\mathbf{d}^{G,n+1} - \mathbf{d}^{G,n}}{\Delta t} \quad \text{and} \quad \mathbf{u}_\Gamma^{n+1} = \frac{\mathbf{d}_\Gamma^{n+1} - \mathbf{d}_\Gamma^{n}}{\Delta t} \tag{23}$$

3. Solve fluid equation with prescribed interface velocity $\mathbf{u}_\Gamma^{n+1}$

$$\mathbf{F}_{II}\mathbf{u}_I^{n+1} = \mathbf{f}_I^F - \mathbf{F}_{I\Gamma}\mathbf{u}_\Gamma^{n+1} \tag{24}$$

for the interior velocity and pressure values $\mathbf{u}_I^{n+1}$ and calculate coupling forces

$$\mathbf{f}_\Gamma^{F,n+1} = \mathbf{F}_{\Gamma I}\mathbf{u}_I^{n+1} + \mathbf{F}_{\Gamma\Gamma}\mathbf{u}_\Gamma^{n+1} \tag{25}$$

4. Solve structural equation loaded with coupling forces $\mathbf{f}_\Gamma^{F,n+1}$

$$\begin{bmatrix} \mathbf{S}_{II} & \mathbf{S}_{I\Gamma} \\ \mathbf{S}_{\Gamma I} & \mathbf{S}_{\Gamma\Gamma} \end{bmatrix} \begin{bmatrix} \mathbf{d}_I^{n+1} \\ \tilde{\mathbf{d}}_\Gamma^{n+1} \end{bmatrix} = \begin{bmatrix} \mathbf{f}_I^S \\ \mathbf{f}_\Gamma^S - (1-\alpha_f)\mathbf{f}_\Gamma^{F,n+1} - \alpha_f \mathbf{f}_\Gamma^n \end{bmatrix} \tag{26}$$

to obtain the structural displacements in the structural fields interior $\mathbf{d}_I^{n+1}$ as well as on the interface $\tilde{\mathbf{d}}_\Gamma^{n+1}$.

To simplify the discussion further the above solution steps are abbreviated with interface operators that map a given interface displacement $\mathbf{d}_\Gamma^{n+1}$ to interface forces as follows

$$\mathbf{f}_\Gamma^{F,n+1} = \mathbf{F}_\Gamma\left(\mathbf{d}_\Gamma^{n+1}\right) \quad \text{and} \quad \mathbf{f}_\Gamma^{S,n+1} = \mathbf{S}_\Gamma\left(\mathbf{d}_\Gamma^{n+1}\right) \tag{27}$$

where the solution demands equilibrium at the interface.

$$\mathbf{F}_\Gamma\left(\mathbf{d}_\Gamma^{n+1}\right) = \mathbf{S}_\Gamma\left(\mathbf{d}_\Gamma^{n+1}\right) \tag{28}$$

The fluid interface operator $\mathbf{f}_\Gamma^{n+1} = \mathbf{F}_\Gamma(\mathbf{d}_\Gamma^{n+1})$ abbreviates steps 2 and 3 of the above algorithm, whereas the inverse structural interface operator $\mathbf{d}_\Gamma^{n+1} = \mathbf{S}_\Gamma^{-1}(\mathbf{f}_\Gamma^{n+1})$ denotes step 4. This way the solver coupling reduces to a single line

$$\tilde{\mathbf{d}}_\Gamma^{n+1} = \mathbf{S}_\Gamma^{-1}(\mathbf{F}_\Gamma(\mathbf{d}_\Gamma^{n+1})). \tag{29}$$

It is understood that this line contains the execution of all three field solvers, one after the other. Each field solver carries its own state and depends on its own initial and boundary conditions in addition to the condition given at the coupling interface.

*Remark 3* With the interface operators (27) defined, the coupling can also be stated based on interface forces

$$\tilde{\mathbf{f}}_\Gamma^{n+1} = \mathbf{F}_\Gamma(\mathbf{S}_\Gamma^{-1}(\mathbf{f}_\Gamma^{n+1})). \tag{30}$$

The resulting algorithm is equivalent to the one based on interface displacements and will not be discussed further. But see [24] for an application of force based couplings.

### 3.2 Fixed-point coupling algorithm

The Dirichlet–Neumann coupling in some sense assumes the structural part to dominate the interaction. If the structure resembles a rigid wall in comparison to the fluid (that is no interaction occurs), the Dirichlet–Neumann assumption is

obvious. If, on the other hand, the structure is very light and flexible, fluid forces will have a huge impact on the structure and the predictor's guess at the interface displacement $\mathbf{d}_\Gamma^{n+1}$ will most probably not match the result.

$$\tilde{\mathbf{d}}_\Gamma^{n+1} \neq \mathbf{d}_\Gamma^{n+1} \tag{31}$$

In these cases an iterative correction of the interface displacement is required. In contrast to a weak coupling scheme that solves the Eq. (29) just once for each time step, iterative or strong coupling schemes iterate (29) until the coupled FSI problem is solved. However, as has been shown in [3,13], a weak coupling Dirichlet–Neumann scheme that couples a flexible structure to an incompressible fluid without subiteration will never be unconditionally stable. The pressure has to be implicitly coupled at least. Thus a strong coupling scheme with iterative correction is mandatory. In the present contribution only fully coupled schemes are considered, however see also [1,29] for iterative coupling methods based on pressure segregation.

The interface operators (29) can be used to define one FSI cycle inside the coupling iteration

$$\tilde{\mathbf{d}}_{\Gamma,i+1}^{n+1} = \mathbf{S}_\Gamma^{-1}(\mathbf{F}_\Gamma(\mathbf{d}_{\Gamma,i}^{n+1})) \tag{32}$$

where $i$ indicates the iteration counter.

*Remark 4* The FSI cycle (32) constitutes one pass in a block Gauß-Seidel solver for the interface displacements. The structural solver $\mathbf{S}_\Gamma^{-1}$ works on the result of the fluid solver $\mathbf{F}_\Gamma$.

In order to define an iterative solver a stopping criteria is required. To this end the interface residual is introduced

$$\mathbf{r}_{\Gamma,i+1}^{n+1} = \tilde{\mathbf{d}}_{\Gamma,i+1}^{n+1} - \mathbf{d}_{\Gamma,i}^{n+1} \tag{33}$$

and as convergence criteria the length scaled square norm of the residual is used.

$$\frac{1}{\sqrt{n_{eq}}} \left| \mathbf{r}_{\Gamma,i+1}^{n+1} \right| < \epsilon \tag{34}$$

For further discussions of the applicable interface norms in FSI calculations see [5].

In order to ensure and accelerate convergence of the iteration a relaxation step is needed after each FSI cycle (32)

$$\begin{aligned} \mathbf{d}_{\Gamma,i+1}^{n+1} &= \mathbf{d}_{\Gamma,i}^{n+1} + \omega_i \mathbf{r}_{\Gamma,i+1}^{n+1} \\ &= \omega_i \tilde{\mathbf{d}}_{\Gamma,i+1}^{n+1} + (1-\omega_i)\mathbf{d}_{\Gamma,i}^{n+1} \end{aligned} \tag{35}$$

with a variable relaxation parameter $\omega_i$. The fixed-point algorithm to solve FSI problems consists of the relaxed FSI cycle (35) with appropriate relaxation parameter and convergence criteria (34). Calculation methods for the relaxation parameter $\omega_i$ will be presented in the next section.

*Remark 5* Equation (35) can be reformulated

$$\begin{aligned} \mathbf{d}_{\Gamma,i+1}^{n+1} &= \omega_i \mathbf{S}_\Gamma^{-1}(\mathbf{F}_\Gamma(\mathbf{d}_{\Gamma,i}^{n+1})) + (1-\omega_i)\mathbf{d}_{\Gamma,i}^{n+1} \\ &= \mathbf{d}_{\Gamma,i}^{n+1} + \omega_i \mathbf{S}_\Gamma^{-1}\left(\mathbf{F}_\Gamma(\mathbf{d}_{\Gamma,i}^{n+1}) - \mathbf{S}_\Gamma(\mathbf{d}_{\Gamma,i}^{n+1})\right) \end{aligned} \tag{36}$$

The formulation (36) constitutes a nonstationary Richardson iteration with the operator $\mathbf{F}_\Gamma - \mathbf{S}_\Gamma$ and the preconditioner $\mathbf{S}_\Gamma^{-1}$. Thus it would be possible to approximate $\mathbf{S}_\Gamma^{-1}$ (see [6]), however this mandates to evaluate $\mathbf{F}_\Gamma - \mathbf{S}_\Gamma$ exactly. In particular the evaluation of the structural solver $\mathbf{S}_\Gamma$ is still required.

*Remark 6* With the interface residual (33) it is possible to define the interface Jacobian

$$\mathbf{J}_\Gamma = \frac{\partial \mathbf{r}_\Gamma}{\partial \mathbf{d}_\Gamma} \tag{37}$$

and apply Newton's method [22] to solve the interface system (28). However, as the interface Jacobian (37) is not easily available, a matrix free Krylov subspace solver [23] has to be applied inside Newton's method. In that case the relaxation step (35) is replaced by the solution of

$$\mathbf{J}_\Gamma \Delta \mathbf{d}_{\Gamma,i+1}^{n+1} = -\mathbf{r}_{\Gamma,i+1}^{n+1} \tag{38}$$

and the update step

$$\mathbf{d}_{\Gamma,i+1}^{n+1} = \mathbf{d}_{\Gamma,i}^{n+1} + \Delta \mathbf{d}_{\Gamma,i+1}^{n+1}. \tag{39}$$

For further discussion of Newton Krylov methods in the context of FSI problems see for instance [10,16].

*Remark 7* Multiple evaluations of the FSI cycle (32) within one time step require field solvers that can be reset to calculate the same time step several times. Black box solvers that cannot be reset are in general not suited for strong coupling FSI calculations.

## 4 Relaxation methods

Relaxation of the interface displacements (35) is nothing but the line search step of a nonlinear solver [17,22]. Consequently the known solver techniques can be applied here as well.

### 4.1 Fixed relaxation parameter

The simplest and most ineffective method is to choose a fixed parameter $\omega$ for all time steps. The relaxation parameter has to be small enough to keep the iteration from diverging, but as large as possible in order to use as much of the new solution as possible and to avoid unnecessary FSI iterations. The optimal $\omega$ value is problem specific and not known a priori. Furthermore even the optimal fixed value will lead to more iterations than a suitable dynamic relaxation parameter.

### 4.2 Aitken relaxation

FSI problems have already been solved in [27,40] using a Dirichlet–Neumann partitioned approach combined with a fixed-point solver based on Aitken's $\Delta^2$ method as given by [20]. This method has proven to be astonishingly simple and efficient.

The central idea of Aitken's $\Delta^2$ method is to use values from two previous iterations to improve the current solution. In the FSI case two pairs of interface displacements $\left(\tilde{\mathbf{d}}_{\Gamma,i+1}, \mathbf{d}_{\Gamma,i}\right)$ and $\left(\tilde{\mathbf{d}}_{\Gamma,i+2}, \mathbf{d}_{\Gamma,i+1}\right)$ are required that fulfill (29). In a scalar case the improved solution could immediately be given

$$d_{\Gamma,i+2} = \frac{d_{\Gamma,i}\tilde{d}_{\Gamma,i+2} - \tilde{d}_{\Gamma,i+1}d_{\Gamma,i+1}}{d_{\Gamma,i} - \tilde{d}_{\Gamma,i+1} - d_{\Gamma,i+1} + \tilde{d}_{\Gamma,i+2}}. \tag{40}$$

This is nothing but one step of the secant method. And with $d_{\Gamma,i+2} = d_{\Gamma,i+1} + \omega_{i+1}\left(\tilde{d}_{\Gamma,i+2} - d_{\Gamma,i+1}\right)$ the relaxation factor becomes

$$\omega_{i+1} = \frac{d_{\Gamma,i} - d_{\Gamma,i+1}}{d_{\Gamma,i} - \tilde{d}_{\Gamma,i+1} - d_{\Gamma,i+1} + \tilde{d}_{\Gamma,i+2}} \tag{41}$$

$$= \omega_i \frac{d_{\Gamma,i} - \tilde{d}_{\Gamma,i+1}}{d_{\Gamma,i} - \tilde{d}_{\Gamma,i+1} - d_{\Gamma,i+1} + \tilde{d}_{\Gamma,i+2}} \tag{42}$$

$$= -\omega_i \frac{r_{\Gamma,i+1}}{r_{\Gamma,i+2} - r_{\Gamma,i+1}} \tag{43}$$

For the vector case the division by $\mathbf{r}_{\Gamma,i+2} - \mathbf{r}_{\Gamma,i+1}$ is of course impossible. Instead [20] suggest to multiply by the vector inverse $\left(\mathbf{r}_{\Gamma,i+2} - \mathbf{r}_{\Gamma,i+1}\right) / \left|\mathbf{r}_{\Gamma,i+2} - \mathbf{r}_{\Gamma,i+1}\right|^2$.

$$\omega_{i+1} = -\omega_i \frac{\left(\mathbf{r}_{\Gamma,i+1}\right)^T \left(\mathbf{r}_{\Gamma,i+2} - \mathbf{r}_{\Gamma,i+1}\right)}{\left|\mathbf{r}_{\Gamma,i+2} - \mathbf{r}_{\Gamma,i+1}\right|^2} \tag{44}$$

This amounts to a projection of the participating vectors in $\mathbf{r}_{\Gamma,i+2} - \mathbf{r}_{\Gamma,i+1}$ direction and to do the scalar extrapolation with the projected values.

*Remark 8* The relaxation parameter calculation (44) is valid in every iteration step. This version has already been used for FSI problems in [27], however a lot of confusion has been caused by citations of [27] that missed the recursion on $\omega_i$ in (44). The Aitken formula without recursion requires two FSI cycles before one relaxation step (44) is possible. This results in a coupling scheme that needs approximately twice the number of iterations to converge.

*Remark 9* The relaxation parameter (44) is exact in linear scalar cases. For vector cases things are not that clear, however, the Aitken relaxation parameter works very well for many FSI problems and is extremely cheap to calculate and to implement.

*Remark 10* Two previous steps are required in (44), thus there is no way to calculate the relaxation parameter after the first FSI cycle $\omega_1^{n+1}$. In [20] it is suggested to use the last $\omega^n$ of the previous time step, however this can sometimes be too large a step already. A better choice is to start with a (problem specific) fixed or at least constrained parameter.

$$\omega_1^{n+1} = \max(\omega^n, \omega_{\max}) \tag{45}$$

*Remark 11* It is possible to use more than two history values to improve the current solution. This idea leads to the known vector extrapolation schemes and will be discussed in a future contribution.

### 4.3 Steepest descent relaxation

The best relaxation parameter possible in (35) is the one that finds the optimal step length in $\mathbf{r}_{\Gamma,i+1}^{n+1}$ direction. To find it the existence of a merit function $\phi(\mathbf{d}_\Gamma)$ is assumed, that is minimal at the solution $\mathbf{d}_\Gamma^{n+1}$ and sufficiently smooth, such that the relaxation parameter $\omega_i$ is given by

$$\omega_i = \arg\min_{\omega_i} \phi(\mathbf{d}_{\Gamma,i}^{n+1} + \omega_i \mathbf{r}_{\Gamma,i+1}^{n+1}). \tag{46}$$

And the condition to determine $\omega_i$ follows

$$\frac{d\phi}{d\omega_i} = \frac{\partial\phi(\mathbf{d}_{\Gamma,i}^{n+1} + \omega_i \mathbf{r}_{\Gamma,i+1}^{n+1})}{\partial \mathbf{d}_\Gamma} \cdot \mathbf{r}_{\Gamma,i+1}^{n+1} \stackrel{!}{=} 0 \tag{47}$$

which leads to

$$\frac{\partial\phi(\mathbf{d}_{\Gamma,i}^{n+1} + \omega_i \mathbf{r}_{\Gamma,i+1}^{n+1})}{\partial \mathbf{d}_\Gamma} = \phi'(\mathbf{d}_{\Gamma,i}^{n+1} + \omega_i \mathbf{r}_{\Gamma,i+1}^{n+1}) \stackrel{!}{=} \mathbf{0}. \tag{48}$$

From a Taylor series expansion of $\phi(\mathbf{d}_\Gamma)$

$$\phi(\mathbf{d}_{\Gamma,i}^{n+1} + \omega_i \mathbf{r}_{\Gamma,i+1}^{n+1}) \approx \phi(\mathbf{d}_{\Gamma,i}^{n+1}) + \omega_i \left(\phi'(\mathbf{d}_{\Gamma,i}^{n+1})\right)^T \mathbf{r}_{\Gamma,i+1}^{n+1} + \frac{\omega_i^2}{2} \left(\mathbf{r}_{\Gamma,i+1}^{n+1}\right)^T \phi''(\mathbf{d}_{\Gamma,i}^{n+1}) \mathbf{r}_{\Gamma,i+1}^{n+1} \tag{49}$$

the expression for the optimal $\omega_i$ is obtained.

$$\omega_i = -\frac{\left(\phi'(\mathbf{d}_{\Gamma,i}^{n+1})\right)^T \mathbf{r}_{\Gamma,i+1}^{n+1}}{\left(\mathbf{r}_{\Gamma,i+1}^{n+1}\right)^T \phi''(\mathbf{d}_{\Gamma,i}^{n+1}) \mathbf{r}_{\Gamma,i+1}^{n+1}} \tag{50}$$

At this point a connection between the merit function $\phi(\mathbf{d}_\Gamma)$ and the interface residual (33) is assumed

$$\phi'(\mathbf{d}_{\Gamma,i}^{n+1}) = \mathbf{r}_{\Gamma,i+1}^{n+1}, \tag{51}$$

an assumption that constrains the admissible interface residuals $\mathbf{r}_{\Gamma,i+1}^{n+1}$ to gradients of a scalar function. A rather severe constraint, that leads to a symmetric interface Jacobian

$$\mathbf{J}_\Gamma = \frac{\partial \mathbf{r}_\Gamma(\mathbf{d}_{\Gamma,i}^{n+1})}{\partial \mathbf{d}_\Gamma} = \phi''(\mathbf{d}_{\Gamma,i}^{n+1}) \tag{52}$$

and the final expression

$$\omega_i = -\frac{\left(\mathbf{r}_{\Gamma,i+1}^{n+1}\right)^T \mathbf{r}_{\Gamma,i+1}^{n+1}}{\left(\mathbf{r}_{\Gamma,i+1}^{n+1}\right)^T \mathbf{J}_\Gamma \mathbf{r}_{\Gamma,i+1}^{n+1}}. \tag{53}$$

Unfortunately the assumption (51) does not hold for the FSI interface residual (33). This is due to the convective term of the Navier-Stokes equation (7) that leads to an unsymmetrical system matrix in the fluid field (15). However the relaxation parameter (53) might still be a very good choice to accelerate the convergence of (32).

*Remark 12* It is perfectly fine to approximate the calculation of the relaxation parameter $\omega_i$. As long as the FSI interface iteration converges, the choice of $\omega_i$ does not affect the solution of the coupled problem. It is just the number of iterations required to reach the solution that depends on $\omega_i$.

The evaluation of (53) with the known residual $\mathbf{r}_{\Gamma,i+1}^{n+1}$ requires the evaluation of the matrix vector product $\mathbf{J}_\Gamma \mathbf{r}_{\Gamma,i+1}^{n+1}$. The interface Jacobian $\mathbf{J}_\Gamma$, however, is not explicitly available. There are means to calculate the matrix vector product exactly [10], but these require specially enhanced fluid solvers. There are two methods, however, that approximate the matrix vector product and can be performed with black box solvers.

#### 4.3.1 Calculation via finite difference

A very simple way to approximate the matrix vector product in (53) is the use of a finite difference

$$\mathbf{J}_\Gamma \mathbf{y} \approx \frac{\mathbf{S}_\Gamma^{-1}(\mathbf{F}_\Gamma(\mathbf{d}_{\Gamma,i}^{n+1} + \delta\mathbf{y})) - \mathbf{d}_{\Gamma,i}^{n+1} - \delta\mathbf{y} - \mathbf{r}_{\Gamma,i+1}^{n+1}}{\delta} \tag{54}$$

with $\delta = \lambda\left(\lambda + \left|\mathbf{d}_{\Gamma,i}^{n+1}\right| / \left|\mathbf{r}_{\Gamma,i+1}^{n+1}\right|\right)$ and a small enough $\lambda$. Here a first order forward difference is reasonable, that builds on the already available residual $\mathbf{r}_{\Gamma,i+1}^{n+1}$ and needs just one more FSI cycle. Still the computational costs are rather high. And the approximation turns out to be numerically sensitive due to the finite difference.

*Remark 13* The numerical cost of (54) can be reduced by avoiding unnecessary accuracy within the nonlinear field solvers. Oftentimes it is sufficient to do just a linear solve for both the fluid and structural field without compromising the accuracy of the approximation.

#### 4.3.2 Calculation via approximated fluid derivatives

Starting from the interface residual (33) and (32) the interface Jacobian applied to a vector is given by

$$\mathbf{J}_\Gamma \mathbf{y} = \left(\mathbf{S}_\Gamma^{-1}\right)'\left(\mathbf{F}_\Gamma(\mathbf{d}_{\Gamma,i}^{n+1})\right) \mathbf{F}'_\Gamma(\mathbf{d}_{\Gamma,i}^{n+1})\,\mathbf{y} - \mathbf{y} \tag{55}$$

where the application of a vector to the derivative of the structural interface operator $\left(\mathbf{S}_\Gamma^{-1}\right)'\left(\mathbf{F}_\Gamma(\mathbf{d}_{\Gamma,i}^{n+1})\right)\mathbf{z}$ is readily available. This operator requires just one linear solver evaluation of the latest structural field linearization. The derivative of the fluid interface operator $\mathbf{z} = \mathbf{F}'_\Gamma(\mathbf{d}_{\Gamma,i}^{n+1})\,\mathbf{y}$, however, posses a problem. This derivative is given by

$$\mathbf{F}'_\Gamma = \frac{d\mathbf{F}_\Gamma}{d\mathbf{d}_\Gamma} = \frac{\partial\mathbf{F}_\Gamma}{\partial\mathbf{d}_\Gamma} + \frac{\partial\mathbf{F}_\Gamma}{\partial\mathbf{u}_\Gamma}\frac{\partial\mathbf{u}_\Gamma}{\partial\mathbf{d}_\Gamma} = \frac{\partial\mathbf{F}_\Gamma}{\partial\mathbf{d}_\Gamma} + \frac{\partial\mathbf{F}_\Gamma}{\partial\mathbf{u}_\Gamma}\frac{1}{\Delta t} \tag{56}$$

according to (18). Unfortunately the derivative $\partial\mathbf{F}_\Gamma/\partial\mathbf{d}_\Gamma$ is not easily available, so it is dropped. This way the influence of the mesh movement on the coupling forces is neglected.

$$\mathbf{F}'_\Gamma \approx \frac{\partial\mathbf{F}_\Gamma}{\partial\mathbf{u}_\Gamma}\frac{1}{\Delta t} \tag{57}$$

The remaining derivative with respect to the fluid velocities is easily available within the fluid solver. So the solution of $\mathbf{z} = \mathbf{F}'_\Gamma(\mathbf{d}_{\Gamma,i}^{n+1})\,\mathbf{y}$ comes down to a linear solve of the fluid field at the current configuration with prescribed interface velocities $\mathbf{y}/\Delta t$.

To clarify things further lets have a look at the limit of (54).

$$\begin{aligned}\mathbf{J}_\Gamma \mathbf{y} &= \lim_{\delta\to 0} \frac{\mathbf{S}_\Gamma^{-1}(\mathbf{F}_\Gamma(\mathbf{d}_{\Gamma,i}^{n+1} + \delta\mathbf{y})) - \mathbf{d}_{\Gamma,i}^{n+1} - \delta\mathbf{y} - \mathbf{r}_{\Gamma,i+1}^{n+1}}{\delta} \\ &\approx \lim_{\delta\to 0} \frac{\mathbf{r}_{\Gamma,i+1}^{n+1} + \mathbf{S}_{\Gamma,lin}^{-1}(\mathbf{F}_{\Gamma,lin}(\delta\mathbf{y})) - \delta\mathbf{y} - \mathbf{r}_{\Gamma,i+1}^{n+1}}{\delta} \\ &\approx \mathbf{S}_{\Gamma,lin}^{-1}(\mathbf{F}_{\Gamma,lin}(\mathbf{y})) - \mathbf{y}\end{aligned} \tag{58}$$

Here everything except the influence of the "small" perturbation $\mathbf{y}$ vanishes, in particular the right hand sides of both field solvers. The remaining field operators are exactly the operator derivatives (55).

*Remark 14* The assumption of a linear addition to the fluid operator $\mathbf{F}_{\Gamma,lin}(\mathbf{y})$ mandates to neglect the derivatives with respect to the interface displacements as discussed above.

## 5 Numerical examples

### 5.1 Driven cavity with flexible bottom

The first example is a simple 2d driven cavity with flexible bottom (Fig. 1) that has already been introduced in [38] and since then has been used for a variety of numerical studies, e.g. [13,27]. There is a unit square cavity with a flexible bottom driven by a prescribed periodical velocity at the top. The fluid domain is discretized with stabilized Q1Q1 elements in an uniform $32 \times 32$ element mesh. At each side there are two unconstrained nodes that allow free in- and outflow of fluid. This way the structural displacements are not constraint by the fluid's incompressibility [24].

The point with this example is its very flexible structure. The structural material is chosen such that the structure's

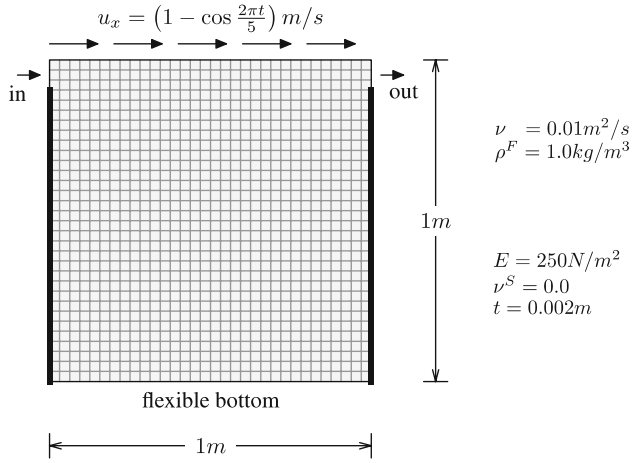


**Fig. 1** Driven cavity with flexible bottom

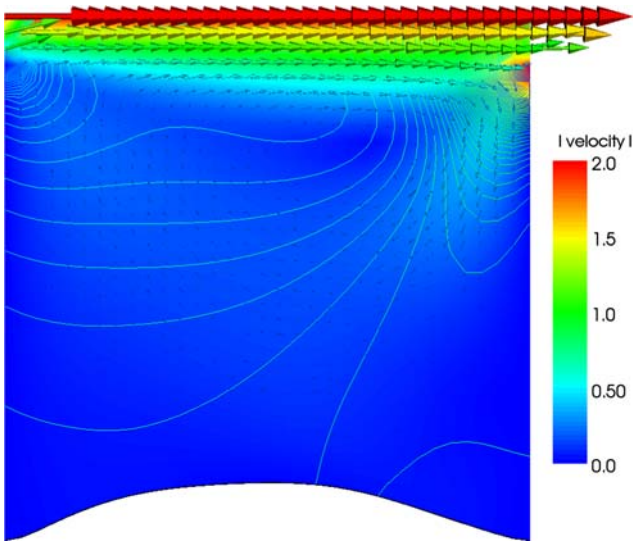


**Fig. 2** Driven cavity velocity and pressure solution at $t = 7.5s$

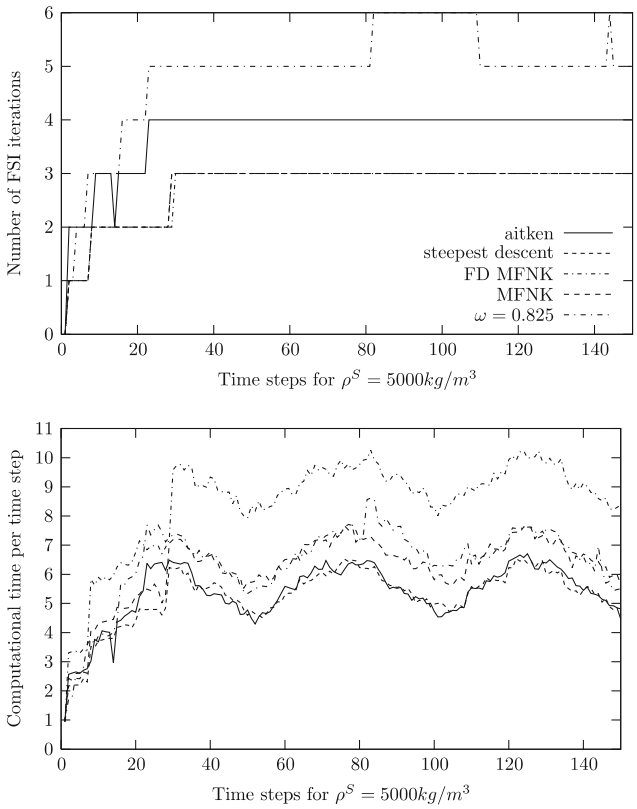


**Fig. 3** Number of FSI iterations and computational time per time step for driven cavity with $\rho^S = 5,000\,\mathrm{kg/m^3}$

main resistance against the fluid pressure stems from its mass, that is its density. This allows to compute a series of test cases with different structural densities that present increasing difficulties to the coupling algorithm.

In all test cases the time step size is $\Delta t = 0.1s$. The tolerance criteria within the nonlinear fluid and structural solvers has been set to the very low value $\epsilon^S = \epsilon^F = 1 \cdot 10^{-10}$ and a direct solver has been applied to the linear field equations. With this precautions (that are only affordable for really small examples) it is guaranteed that the convergence rate of the FSI iteration is not limited by inexact field solvers. The convergence tolerance at the FSI interface (34) is set to $\epsilon = 1 \cdot 10^{-7}$.

Figure 2 shows the fluid domain deformation, the fluid velocity norm and isolines of the fluid pressure at time level $t = 7.5$ s. The velocity vectors at the top of the cavity are the prescribed boundary conditions.

The problem has among others been solved with Aitken relaxation, steepest descent relaxation and a fixed relaxation parameter $\omega = 0.825$. This value for the fixed $\omega$ has been found by trial and error to be the best choice in the second set of example calculations. The maximum allowed start relaxation for the Aitken method (45) has been set to $\omega_{\max} = 0.1$. For the steepest descent relaxation calculation the evaluation of the interface Jacobian (37) multiplied with the interface residual is based on field solver derivatives (55) as suggested in [27].

For comparison Newton's method with a matrix free solver has also been used on the nonlinear interface equation (33). Both versions of the matrix vector product approximation, the finite difference (54) with $\lambda = 1 \cdot 10^{-4}$ and the evaluation based on field solver derivatives (55), have been applied. These versions are labeled FD MFNK and MFNK, respectively. In the second residual evaluation in the finite difference approximation (54) the field solvers are restricted to just one linear solve to save computation time. See [10,15,16] for algorithmic details of the Newton Krylov method for FSI problems.

The first set of runs, shown in Fig. 3, with a structural density of $\rho^S = 5,000\,\mathrm{kg/m^3}$ show an interesting coincidence as most coupling methods require three FSI iterations.

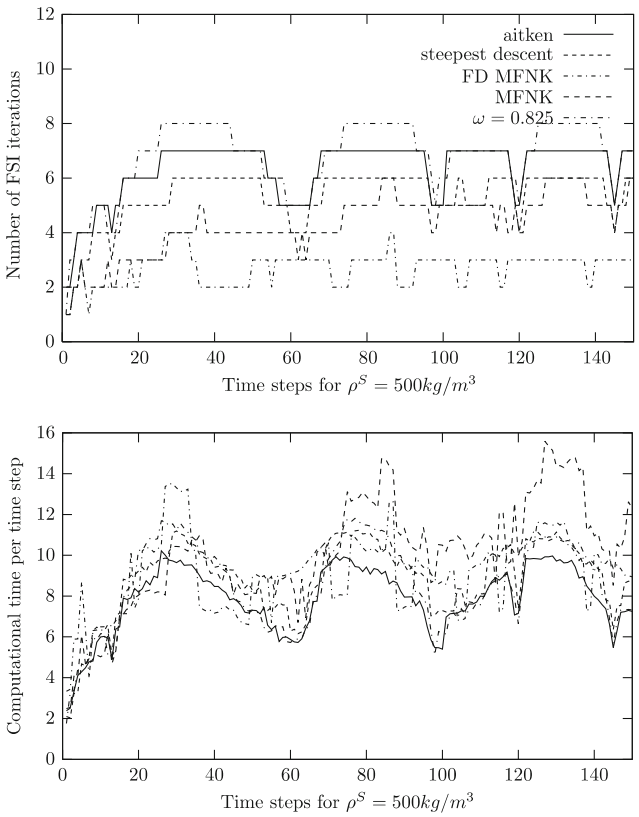


**Fig. 4** Number of FSI iterations and computational time per time step for driven cavity with $\rho^S = 500\,\mathrm{kg/m^3}$

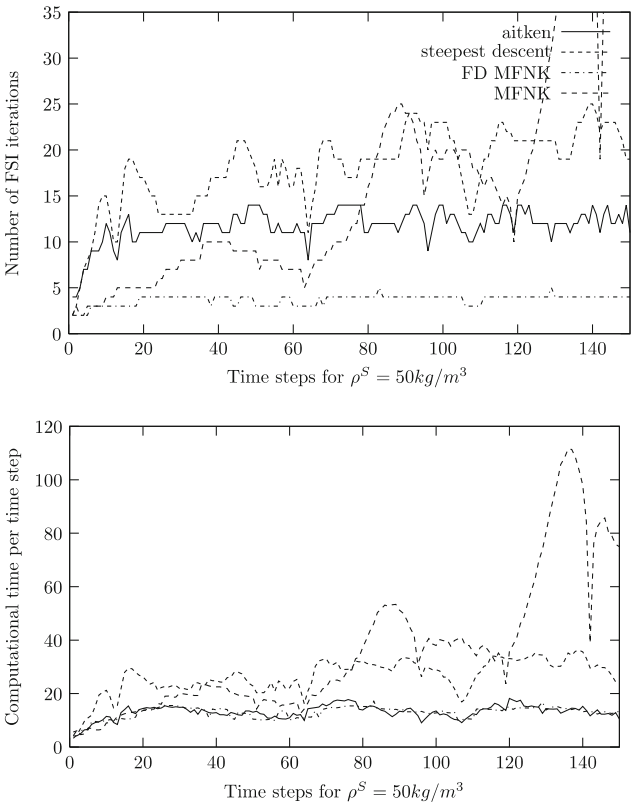


**Fig. 5** Number of FSI iterations and computational time per time step for driven cavity with $\rho^S = 50\,\mathrm{kg/m^3}$

Exceptions are the coupling method with a fixed relaxation parameter and the one with Aitken's parameter. The time required per iteration, however, is different for different methods. The very cheap Aitken method, that needs nothing more than one FSI cycle per iteration, requires about the same computational time as the method of steepest descent. The slowest method here is the matrix free Newton Krylov method based on finite differences, that needs a lot more interface residual evaluations per FSI iteration.

These and all following timings have been done on a dual head Opteron node with a MPI based code executed on both processors. The time measured is the execution time of the coupling solver. Of course these timings are to be taken with a pinch of salt, the general picture is very well represented but small variation that can occur in multiple runs of the same problem are not accounted for.

Decreasing the structural density to $\rho^S = 500\,\mathrm{kg/m^3}$ results in increased work for the coupling algorithms, see Fig. 4. Now the Newton Krylov methods require less iterations than the fixed point methods, however the neglection of the fluid field's dependence on the mesh movement in the Newton Krylov method leads to a noticeable increase of iterations. Timings show that the amount of work has indeed increased for all coupling methods and there is no tremendous difference in the computational time required between different methods. The fastest ones are now the Aitken method and the finite difference based Newton Krylov method.

A final decrease to $\rho^S = 50\,\mathrm{kg/m^3}$, Fig. 5, leads to a diverging relaxation method with fixed parameter. This could be cured, of course, by choosing a smaller $\omega$, however as this is not a recommended method anyway, it is dropped at this point. Two further points to notice are that the Aitken method gains a definite advantage over the method of steepest descent and the approximated Newton Krylov method does not seem to do very well after the first prescribed velocity period.

Timings confirm this picture and interesting enough the Aitken method and the finite difference based Newton Krylov method are again close up. A further decrease of the structural density, however, would eventually lead to a problem that the Newton Krylov method solves faster than the Aitken method.

For further insight into the behavior of the fixed-point coupling algorithm a look at the behavior of the relaxation parameter $\omega_i$ during a particular time step might be of use. As an example we choose step 31 in the $\rho^S = 50\,\mathrm{kg/m^3}$ series. In this step the number of iterations required is very similar in the Aitken and steepest descent methods. See Fig. 6.

As a matter of fact the relaxation parameter varies a lot during one FSI interaction. In particular the Aitken version does not seem to follow a definite pattern. The steepest descent

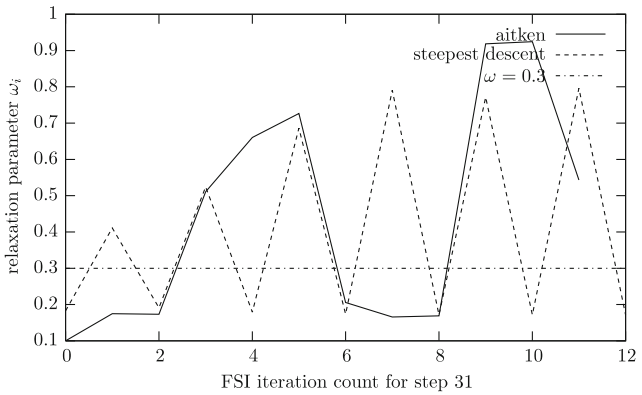


**Fig. 6** Relaxation parameter $\omega_i$ for time step 31 in the $\rho^S = 50\,\mathrm{kg/m^3}$ case

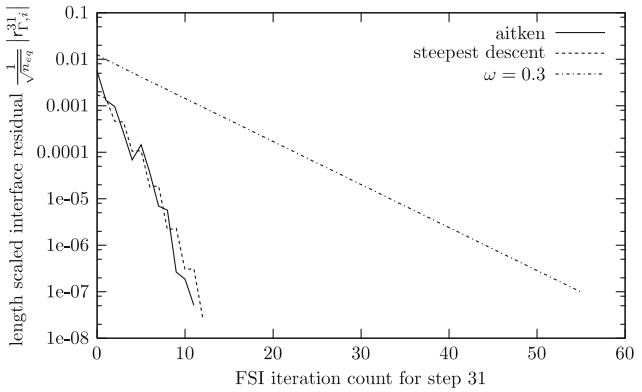


**Fig. 7** Residual $\mathbf{r}^{31}_{\Gamma,i}$ for time step 31 in the $\rho^S = 50\,\mathrm{kg/m^3}$ case

parameter, on the other hand, does show a curious behavior as there seems to be a lower limit that is touched in every other step.

A look at the interface residual norm in Fig. 7 reveals, that the method of steepest descent seems to enjoy a residual reduction only with its $\omega_i$ peak values. Overall, however, both methods perform comparable in this time step. In contrast the run with fixed relaxation parameter $\omega_i = 0.3$ requires substantially more iterations. With the fixed parameter $\omega_i = 0.4$, however, the simulation did break down before step 31.

### 5.2 Pressure wave in flexible tube

The second example is a 3d flow in a flexible tube as it has been presented in [10,15]. The example is motivated by the type of problem encountered in hemodynamics. The tube has a length of $l = 5\,\mathrm{cm}$, a inner radius of $r_i = 0.5\,\mathrm{cm}$ and an outer radius of $r_o = 0.6\,\mathrm{cm}$. The structural density is $\rho^S = 1.2\,\mathrm{g/cm^3}$. A Saint Venant-Kirchhof material is used with Young modulus $E = 3 \cdot 10^6\,\mathrm{dynes/cm^2}$ and Poisson ratio $\nu^S = 0.3$. The fluid has a viscosity $\mu = 0.03$ Poise and a density $\rho^F = 1.0\,\mathrm{g/cm^3}$. The time step size used for the simulations is $\Delta t = 0.0001\,\mathrm{s}$.

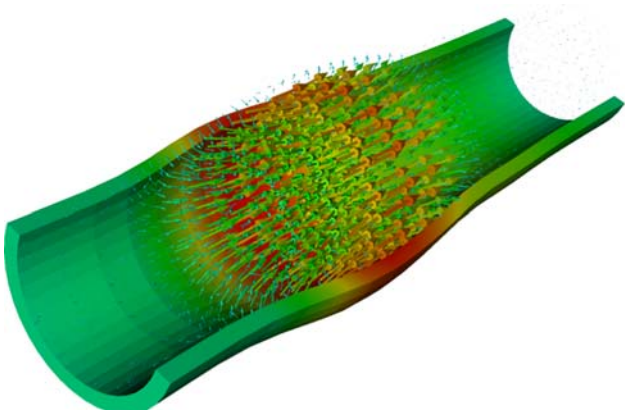

**Fig. 8** Flexible tube with 10 times enlarged deformations and velocities at $t = 0.0055\,\mathrm{s}$

The tube is fixed at both ends. The fluid is initially at rest and loaded with a traction of $1.3332 \cdot 10^4\,\mathrm{dynes/cm^2}$ for $3 \cdot 10^{-3}\,\mathrm{s}$. As a result a pressure wave travels along the tube.

The deformation of the tube at $t = 0.0055\,\mathrm{s}$, ten times enlarged, is shown in Fig. 8 together with corresponding velocity values.

For this example the steepest descent method performed very badly. Acceptable results have been obtained from the Aitken method and the two Newton Krylov methods (38) explained above.

As can be seen in Fig. 9 the Newton Krylov method based on finite differences is by far the fastest method in this case. In comparison to [10], however, the Aitken method requires only a moderate number of iterations and only needs approximately 1.5 times the computational time of the fastest Newton Krylov method. A possible reason is that in [10] a less effective version of the Aitken method is used.

*Remark 15* In order to gain meaningful comparisons all example calculations employ the very simple interface predictor

$$\mathbf{d}^{n+1}_{\Gamma,0} = \mathbf{d}^{n}_{\Gamma}. \tag{59}$$

A more elaborated predictor can cause a tremendous speedup of the FSI iteration.

## 6 Conclusion

The fixed-point FSI solver with relaxation introduced in [40] has been revisited. This solver stood the test of time very well. The main advantage of fixed-point FSI solvers based on a Dirichlet–Neumann partitioning is the simple implementation with available field solvers. The calculation of a specific relaxation parameter in each iteration step proved to be crucial. This new presentation contains all details of the

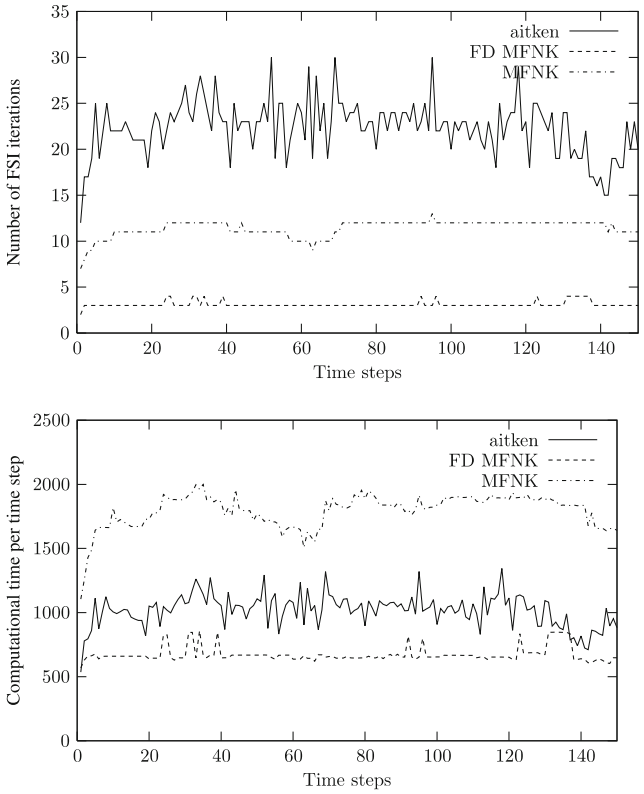


**Fig. 9** Number of FSI iterations and computational time per time step for pressure wave in flexible tube calculation

coupled FSI solver. Recent FSI developments are taken into account. The relaxation based fixed-point solvers are shown to be just one option in a general solver framework for interface coupled problems. Comparisons with related Newton based FSI solvers are make. The proposed relaxation methods compare very well, even with much more elaborated FSI solvers based on Newton Krylov methods. In particular the Aitken relaxation method as proposed by [20] shows very good convergence properties at surprisingly low cost. This method has often been underestimated in the last years due to an unfortunate misinterpretation of the original proposals [27,40].

**Acknowledgments** The authors would like to thank Daniel P. Mok, who did the major part of the work on relaxation methods for fixed-point FSI solvers during his PhD time, that has been supervised by W.A. Wall at the Institute for Structural Mechanics of the University of Stuttgart under the direction of E. Ramm.

## References

1. Badia S, Codina R (2007) On some fluid–structure iterative algorithms using pressure segregation methods. application to aeroelasticity. Int J Numer Methods Eng 72(1):46–71
2. Bazilevs Y, Calo VM, Zhang Y, Hughes TJR (2006) Isogeometric fluid–structure interaction analysis with applications to arterial blood flow. Comput Mech 38(4–5):310–322
3. Causin P, Gerbeau J-F, Nobile F (2005) Added-mass effect in the design of partitioned algorithms for fluid-structure problems. Comput Methods Appl Mech Eng 194:4506–4527
4. Chung J, Hulbert GM (1993) A time integration algorithm for structural dynamics with improved numerical dissipation: the generalized-$\alpha$ method. J Appl Math 60:371–375
5. Deparis S (2004) Numerical analysis of axisymmetric flows and methods for fluid–structure interaction arising in blood flow simulation. Dissertation, EPFL
6. Deparis S, Discacciati M, Fourestey G, Quarteroni A (2006) Fluid–structure algorithms based on Steklov-Poincaré operators. Comput Methods Appl Mech Eng 195:5797–5812
7. Dettmer WG, Peric D (2006) A computational framework for fluid–structure interaction: finite element formulation and applications. Comput Methods Appl Mech Eng 195:5754–5779
8. Farhat C (2004) CFD-based nonlinear computational aeroelasticity. In: Stein E, De Borst R, Hughes TJR (eds) Encyclopedia of Computational mechanics, vol 3, chap. 13. Wiley, NY
9. Farhat C, Geuzaine P (2004) Design and analysis of robust ale time-integrators for the solution of unsteady flow problems on moving grids. Comput Methods Appl Mech Eng 193:4073–4095
10. Fernández MÁ, Moubachir M (2005) A Newton method using exact jacobians for solving fluid–structure coupling. Comput Struct 83(2–3):127–142
11. Förster Ch (2007) Robust methods for fluid–structure interaction with stabilised finite elements. Dissertation, Institut für Baustatik und Baudynamik Universität Stuttgart
12. Förster Ch, Wall WA, Ramm E (2005) On the geometric conservation law in transient flow calculations on deforming domains. Int J Numer Methods Fluids 50:1369–1379
13. Förster Ch, Wall WA, Ramm E (2007) Artificial added mass instabilities in sequential staggered coupling of nonlinear structures and incompressible viscous flows. Comput Methods Appl Mech Eng 196:1278–1293
14. Förster Ch, Wall WA, Ramm E (2008) Stabilized finite element formulation for incompressible flow on distorted meshes. Int J Numer Methods Fluids (in press)
15. Gerbeau J-F, Vidrascu M (2003) A quasi-Newton algorithm based on a reduced model for fluid–structure interaction problems in blood flows. Math Model Numer Anal 37(4):631–647
16. Gerbeau J-F, Vidrascu M, Frey P (2005) Fluid–structure interaction in blood flows on geometries coming from medical imaging. Comput Struct 83:155–165
17. Golub GH, Van Loan CF (1996) Matrix computations, 3rd edn. The Johns Hopkins University Press, Baltimore
18. Heil M (2004) An efficient solver for the fully coupled solution of large-displacement fluid–structure interaction problems. Comput Methods Appl Mech Eng 193:1–23
19. Hübner B, Walhorn E, Dinkler D (2004) A monolithic approach to fluid–structure interaction using space-time finite elements. Comput Methods Appl Mech Eng 193:2087–2104
20. Irons B, Tuck RC (1969) A version of the Aitken accelerator for computer implementation. Int J Numer Methods Eng 1:275–277
21. Kalro V, Tezduyar TE (2000) A parallel 3d computational method for fluid–structure interactions in parachute systems. Comput Methods Appl Mech Eng 190:321–332
22. Kelley CT (1995) Iterative Methods for linear and nonlinear equations frontiers in applied mathematics. SIAM
23. Knoll DA, Keyes DE (2004) Jacobian-free Newton-Krylov methods: a survey of approaches and applications. J Comput Phys 193:357–397
24. Küttler U, Förster Ch, Wall WA (2006) A solution for the incompressibility dilemma in partitioned fluid–structure interaction with pure Dirichlet fluid domains. Comput Mech 38:417–429
25. Matthies HG, Steindorf J (2003) Partitioned strong coupling algorithms for fluid–structure interaction. Comput Struct 81:805–812

26. Michler C, van Brummelen EH, de Borst R (2005) An interface Newton-Krylov solver for fluid–structure interaction. Int J Numer Methods Fluids 47:1189–1195
27. Mok DP, Wall WA (2001) Partitioned analysis schemes for the transient interaction of incompressible flows and nonlinear flexible structures. In: Wall WA, Bletzinger K-U, Schweitzerhof K (eds) Trends in computational structural mechanics,
28. Park KC, Felippa CA, Ohayon R (2001) Partitioned formulation of internal fluid–structure interaction problems by localized Lagrange multipliers. Comput Methods Appl Mech Eng 190(24–25):2989–3007
29. Quaini A, Quarteroni A (2007) A semi-implicit approach for fluid–structure interaction based on an algebraic fractional step method. Math Models Methods Appl Sci 17(6):957–983
30. Le Tallec P, Mouro J (2001) Fluid structure interaction with large structural displacements. Comput Methods Appl Mech Eng 190(24–25):3039–3067
31. Tezduyar TE (2007) Finite elements in fluids: Special methods and enhanced solution techniques. Comput Fluids 36:207–223
32. Tezduyar TE (2007) Finite elements in fluids: stabilized formulations and moving boundaries and interfaces. Comput Fluids 36:191–206
33. Tezduyar TE, Sathe S (2007) Modelling of fluid–structure interactions with the space-time finite elements: solution techniques. Int J Numer Meth Fluids 54(6–8):855–900
34. Tezduyar TE, Sathe S, Cragin T, Nanna B, Conklin BS, Pausewang J, Schwaab M (2007) Modelling of fluid–structure interactions with the space-time finite elements: arterial fluid mechanics. Int J Numer Meth Fluids 54(6–8):901–922
35. Tezduyar TE, Sathe S, Keedy R, Stein K (2006) Space-time finite element techniques for computation of fluid–structure interactions. Comput Methods Appl Mech Eng 195:2002–2027
36. Tezduyar TE, Sathe S, Stein K (2006) Solution techniques for the fully-discretized equations in computation of fluid–structure interactions with the space–time formulations. Comput Methods Appl Mech Eng 195:5743–5753
37. Vierendeels J (2005) Implicit coupling of partitioned fluid–structure interaction solvers using a reduced order model. AIAA Fluid Dyn Conf Exhib 35:1–12
38. Wall WA (1999)Fluid-Struktur-Interaktion mit stabilisierten Finiten Elementen. Dissertation, Institut für Baustatik, Universität Stuttgart
39. Wall WA, Gerstenberger A, Gamnitzer P, Förster Ch, Ramm F (2006) Large deformation fluid–structure interaction—advances in ALE methods and new fixed grid approaches. In: Bungartz H-J, Schäfer M (eds) Fluid–structure interaction: modelling, simulation, optimisation, LNCSE. Springer, Heidelberg
40. Wall WA, Mok DP, Ramm E (1999) Partitioned analysis approach of the transient coupled response of viscous fluids and flexible structures. In: Wunderlich W (Ed.), Solids, structures and coupled problems in engineering, proceedings of the European conference on computational mechanics ECCM '99, Munich
41. Wüchner R, Kupzok A, Bletzinger K-U (2007) A framework for stabilized partitioned analysis of thin membrane-wind interaction. Int J Numer Methods Fluids 54(6–8)